JP Journal of Heat and Mass Transfer

https://pphmjopenaccess.com
https://doi.org/10.17654/0973576326007
Volume 39, Number 1, February 2026, Pages 121-138
P-ISSN: 0973-5763
E-ISSN: 3049-2556

SENSITIVITY ANALYSIS OF THE TERNARY HYBRID NANOFLUID FLOW PAST A PERMEABLE CYLINDER

Umi Nadrah Hussein[1], Najiyah Safwa Khashi'ie[1,*], Mohd Fariduddin Mukhtar[2], Didit Adytia[3] and Mohamad Rafiezi Mat Zainu Zaman[4]

[1]Fakulti Teknologi dan Kejuruteraan Mekanikal
Universiti Teknikal Malaysia Melaka
76100 Durian Tunggal
Melaka, Malaysia
e-mail: najiyah@utem.edu.my

[2]Fakulti Pengurusan Teknologi Dan Teknousahawanan
Universiti Teknikal Malaysia Melaka
76100 Durian Tunggal
Melaka, Malaysia

[3]School of Computing
Telkom University
Bandung, 40257, Indonesia

Received: December 25, 2025; Accepted: January 28, 2026

Keywords and phrases: ternary hybrid nanofluid, heat transfer, skin friction, magnetic field, response surface methodology, sensitivity analysis.

*Corresponding author

How to cite this article: Umi Nadrah Hussein, Najiyah Safwa Khashi'ie, Mohd Fariduddin Mukhtar, Didit Adytia and Mohamad Rafiezi Mat Zainu Zaman, Sensitivity analysis of the ternary hybrid nanofluid flow past a permeable cylinder, JP Journal of Heat and Mass Transfer 39(1) (2026), 121-138. https://doi.org/10.17654/0973576326007

Published Online: February 6, 2026

[4]Microtech Devices Sdn Bhd
Pusat Perdagangan KLH, Menara KLH
Bandar Puchong Jaya, 47100 Puchong
Selangor, Malaysia

Abstract

This numerical study highlights the sensitivity analysis of the ternary copper-alumina-titania/water hybrid nanofluid flow over a permeable cylinder under the influence of magnetic field (MHD), curvature parameter and velocity slip. The governing boundary layer and energy equations are simplified and numerically solved using the bvp4c solver available in Matlab. Meanwhile, the response surface methodology (RSM) and sensitivity analysis are employed using Minitab software to assess the contribution and significance of these physical factors on the selected responses, namely, heat transfer and skin friction coefficients. The findings indicate that velocity slip (factor *C*) has the most dominant influence on heat transfer enhancement, while curvature (factor *B*) is the primary determinant of the skin friction coefficient. Moreover, interaction effects, particularly *BC* (combination of curvature and velocity slip factors) and *AC* (combination of magnetic parameter and velocity slip factors), significantly impact the flow behaviour, emphasizing the importance of considering coupled parameter interactions for optimizing system performance. The results highlight the practical implications of these findings in heat exchangers, industrial cooling systems, and thermal management technologies, where precise control of flow and heat transfer is crucial.

1. Introduction

A nanofluid can be produced by dispersing metallic or non-metallic nanoparticles or nanofibers with a typical size of less than 100 nm in a base liquid. With the increasing demand for technological advancements, optimizing heat transfer efficiency has emerged as a crucial area of research, driving the development and exploration of hybrid nanofluids. Numerous studies, including those by Sheremet et al. [1-3], Babazadeh et al. [4], Zhang et al. [5], Devi and Devi [6-8], Takabi and Salehi [9], along with several

comprehensive review articles [10-14], have extensively examined hybrid nanofluids across diverse thermal and fluid flow conditions. Ternary hybrid nanofluids, which incorporate three different types of nanoparticles, offer enhanced control over thermal conductivity, viscosity, and stability, further extending the advantages of hybrid nanofluids. Jamrus et al. [15] investigated a copper-alumina-titania/water ternary nanofluid and observed that increasing titania concentration led to an improvement in heat transfer rate. A fundamental Hiemenz flow model for ternary hybrid nanofluids past a stretching/shrinking sheet was further explored by Jamrus et al. [16], where they compared the skin friction and heat transfer coefficients of hybrid (Cu-Al_2O_3) and ternary hybrid (Cu-Al_2O_3-TiO_2) nanofluids. Their results indicated that the ternary hybrid nanofluid exhibited superior skin friction and heat transfer characteristics compared to its hybrid counterpart. Very recently, Hussein et al. [17, 18] studied the MHD flow of ternary nanofluid (copper-alumina-titania/water) past a permeable cylinder with velocity slip and Joule heating effect, correspondingly.

Beyond numerical computation, experimental design provides significant advantages in analyzing complex fluid flow phenomena involving multiple interacting parameters. In fluid dynamics research, Mehmood et al. [19] explored the application of RSM and ANOVA in studies involving rotating disks, while several other studies [20-22] successfully utilized these techniques to optimize heat transfer efficiency and flow stability in various fluid systems. This study is designed to achieve two primary objectives. First, it aims to generate comprehensive numerical solutions for the governing model, ensuring that all possible solution branches are captured. Second, it employs RSM and statistical analysis to gain a deeper understanding of fluid flow characteristics and response behaviours. To achieve these goals, the governing partial differential equations are converted into a system of ordinary differential equations (ODEs) through similarity transformation. The statistical analysis is carried out using Minitab software's general linear model fit, while the central composite design (CCD) approach in RSM is applied to determine an optimized dataset for evaluation.

2. Mathematical Formulation

The steady-state flow of ternary hybrid nanofluid, consisting of copper-alumina-titania nanoparticles dispersed in water, along with heat transfer around a permeable cylindrical structure of radius a, is illustrated in Hussein et al. [17]. The fluid motion is restricted to $r \geq 0$, and the azimuthal coordinate φ is defined transversely, with $\partial/\partial\varphi = 0$ ensuring axial symmetry. The velocity profile of the shrinking cylinder is expressed in a specific functional form $\lambda U_w(x) + U_{\text{slip}}$, where $U_w(x) = u_0 x/L$, while the velocity slip condition is introduced as a governing parameter with $U_{\text{slip}} = A_0\, \partial u/\partial r$. The surrounding fluid maintains a constant temperature of T_∞ whereas the surface temperature of the cylinder follows a variable distribution given by a predefined function $T_w = T_\infty + T_0(x/L)^2$, where the characteristic temperature and constant parameters are denoted as T_0 and m, accordingly.

By incorporating the boundary layer approximations and adopting the Tiwari and Das [23] model to characterize the ternary hybrid nanofluid, the governing physical system is represented through a set of partial differential equations (PDEs) as outlined in Hussein et al. [17, 18]. These equations describe the momentum and thermal transport mechanisms within the fluid domain, considering the interactions between copper, alumina, and titania nanoparticles suspended in the base fluid (water). The formulation accounts for the effects of viscosity, thermal conductivity, and nanoparticle volume fraction, ensuring a comprehensive mathematical representation of the fluid behavior around the permeable shrinking cylinder.

Continuity equation:

$$\frac{\partial u}{\partial x} + \frac{\partial v}{\partial r} = 0, \tag{1}$$

Momentum equation:

$$u\frac{\partial u}{\partial x} + v\frac{\partial u}{\partial r} = \frac{\mu_{thnf}}{\rho_{thnf}}\left(\frac{\partial^2 u}{\partial r^2} + \frac{1}{r}\frac{\partial u}{\partial r}\right) - \frac{\sigma_{thnf} B_0^2}{\rho_{thnf}} u, \tag{2}$$

Energy equation:

$$u\frac{\partial T}{\partial x}+v\frac{\partial T}{\partial r}=\frac{k_{thnf}}{(\rho C_p)_{thnf}}\left(\frac{\partial^2 T}{\partial r^2}+\frac{1}{r}\frac{\partial T}{\partial r}\right), \tag{3}$$

$$u=\lambda U_w+A_0\frac{\partial u}{\partial r},\ v=v_w,\ T=T_w,\ \text{at}\ r=a,$$

$$u\to 0,\ T\to T_\infty,\ \text{as}\ r\to\infty. \tag{4}$$

Here, u and v represent the velocity components along the x- and r-directions, respectively. The stretching/shrinking parameter λ determines the nature of the cylinder's motion, where a negative value corresponds to a shrinking surface, a positive value indicates stretching, and a zero value represents an immobile surface. The thermophysical properties of ternary hybrid nanofluid can be found in Hussein et al. [17, 18]. The parameters ϕ_1, ϕ_2 and ϕ_3 denote the volume fractions of alumina, copper, and titania nanoparticles, respectively. Specific cases of the nanofluid composition can be obtained by adjusting these volume fractions: setting $\phi_3 = 0$ results in a copper-alumina/water nanofluid, $\phi_1 = \phi_3 = 0$ corresponds to a copper-water nanofluid, $\phi_2 = \phi_3 = 0$ leads to an alumina-water nanofluid, and $\phi_1 = \phi_2 = 0$ describes a titania-water nanofluid. The thermophysical properties of the individual nanoparticles and the base fluid are summarized in Table 1.

The appropriate similarity transformations that satisfy the continuity equation (1) for the steady flow of a ternary hybrid nanofluid over a permeable shrinking/stretching cylinder are typically introduced to reduce the governing PDEs into a set of ODEs. A common form of similarity variables for this type of flow problem is:

$$\eta=\sqrt{\frac{u_0}{\nu_f L}}\frac{r^2-a^2}{2a},\quad u=\frac{u_0 x}{L}f'(\eta),$$

$$v=-\frac{a}{r}\sqrt{\frac{u_0\nu_f}{L}}f(\eta),\quad \theta(\eta)=\frac{T-T_\infty}{T_w-T_\infty}. \tag{5}$$

Table 1. Thermophysical properties of the selected particles

Physical properties	Al_2O_3	Cu	TiO_2	Water
C_p (J/kgK)	765	385	686.2	4179
ρ (kg/m^3)	3970	8933	4250	997.1
k (W/mK)	40	400	8.9538	0.6130
σ (s/m)	35×10^6	59.6×10^6	2.6×10^6	5.5×10^{-6}

Meanwhile, the mass flux velocity in equation (4) is represented by $v_w = -\frac{a}{r}\sqrt{\frac{u_0 \nu_f}{L}}S$, where $S > 0$ denotes the suction parameter. After applying the similarity transformation, the fundamental equations presented in equations (2) and (3), along with the boundary conditions specified in equation (5), are transformed into a reduced system of ODEs. This reduction simplifies the governing equations, facilitating their numerical within the framework of the ternary hybrid nanofluid model.

$$\frac{\mu_{thnf}/\mu_f}{\rho_{thnf}/\rho_f}[(1+2\eta\gamma)f''' + 2\gamma f''] + f f'' - f'^2 - \frac{\sigma_{thnf}/\sigma_f}{\rho_{thnf}/\rho_f}Mf' = 0, \quad (6)$$

$$\frac{1}{Pr}\frac{k_{thnf}/k_f}{(\rho C_p)_{thnf}/(\rho C_p)_f}[(1+2\gamma\eta)\theta'' + 2\gamma\theta'] + f\theta' - 2f'\theta = 0, \quad (7)$$

$$f(0) = S, \quad f'(0) = \lambda + Kf''(0), \quad \theta(0) = 1,$$

$$f'(\infty) \to 0, \quad \theta(\infty) \to 0. \quad (8)$$

In this formulation, $\gamma = \sqrt{\nu_f L/u_0 a^2}$ represents the curvature parameter, where $\gamma = 0$ corresponds to the case of a stretching/shrinking flat plate. The dimensionless parameter $Pr = (\mu C_p)_f/k_f$ denotes the Prandtl number, which characterizes the relative influence of momentum and thermal diffusivities. The term $M = \sigma_f B_0^2/c\rho_f$ signifies the magnetic parameter, indicating the impact of an applied magnetic field on the fluid flow.

Additionally, $K = A_0\sqrt{u_0/L\nu_f}$ denotes the velocity slip parameter, which accounts for the slip condition at the boundary. The skin friction coefficient and the local Nusselt number are the dimensionless quantities which provide insight into the fluid flow characteristics and thermal performance of the ternary hybrid nanofluid over the permeable shrinking /stretching cylinder and given by (see Hussein et al. [17, 18]):

$$Re_x^{1/2}C_f = \frac{\mu_{thnf}}{\mu_f} f''(0), \quad Re_x^{-1/2}Nu_x = -\frac{k_{thnf}}{k_f}\theta'(0), \tag{9}$$

where $Re_x = xU_w/\nu_f$ is the local Reynolds number.

3. Response Surface Methodology and Sensitivity Analysis

This section provides a detailed discussion on the computational findings obtained by solving equations (6)-(8) utilizing MATLAB's bvp4c solver. The evaluation emphasizes the influence of multiple physical parameters associated with the formulated model, where parameter values are adopted from the previous research conducted by Hussein et al. [17] such that $S = 3.1$, $Pr = 6.2$ and $\phi_1 = \phi_2 = \phi_3 = 0.01$. Since present work is a continuation work by Hussein et al. [17], only the findings from response surface and sensitivity analysis are highlighted. Statistical analysis is employed to pinpoint the factors that significantly enhance these responses. Table 2 presents the RSM using the central composite design, which involves 20 experimental trials across three variables. The magnetic, couple stress, and suction parameters are referred to as factors *A*, *B*, and *C*, respectively, such that low (–1), medium (0), and high (+1) levels reflect their different magnitudes. The numerical solutions in Table 3 are computed from the MATLAB's bvp4c solver. Meanwhile, a general response surface equation (see equation (10)) contains the intercept (r_0), as well as the mix interaction (r_{AB}, r_{BC}, r_{CA}), linear (r_A, r_B, r_C) and quadratic $(r_{A^2}, r_{B^2}, r_{C^2})$ effects.

These coefficients are obtained from the response surface analysis.

$$y = r_0 + r_A A + r_B B + r_C C + r_{AB} AB + r_{CA} CA + r_{BC} BC + r_{A^2} A^2 + r_{B^2} B^2 + r_{C^2} C^2 + \varepsilon. \quad (10)$$

Table 2. Experimental design with RSM

Run	Real			Coded				
	M	γ	K	A	B	C	Skin Friction Coefficient	Heat Transfer Coefficient
1	0.1	0	0.1	1	-1	1	5.516665964	16.699281945
2	0.05	0.05	0.05	0	0	0	5.258150874	16.830213545
3	0	0	0.1	-1	-1	1	5.321248084	16.684022458
4	0	0.05	0.05	-1	0	0	5.162216080	16.822854049
5	0.05	0.05	0.1	0	0	1	5.298319062	16.662318040
6	0.1	0.05	0.05	1	0	0	5.347752901	16.837018614
7	0.05	0.1	0.05	0	1	0	5.151607970	16.803842236
8	0	0.1	0	-1	1	-1	4.999573160	16.944157580
9	0.05	0.05	0.05	0	0	0	5.258150874	16.830213545
10	0.05	0	0.05	0	-1	0	5.346566125	16.854235320
11	0.05	0.05	0.05	0	0	0	5.258150874	16.830213545
12	0.05	0.05	0	0	0	-1	5.170899480	16.973080115
13	0.1	0.1	0	1	1	-1	5.178543967	16.957599541
14	0	0	0	-1	-1	-1	5.168049778	16.988587381
15	0.05	0.05	0.05	0	0	0	5.258150874	16.830213545
16	0	0.1	0.1	-1	1	1	4.963526676	16.612924417
17	0.1	0	0	1	-1	-1	5.306680377	16.998250687
18	0.05	0.05	0.05	0	0	0	5.258150874	16.830213545
19	0.1	0.1	0.1	1	1	1	5.279539661	16.640310441
20	0.05	0.05	0.05	0	0	0	5.258150874	16.830213545

Figures 1 and 2 show the Pareto charts of standardized effects illustrating the impact of factors A (magnetic parameter), B (curvature parameter), and C (velocity slip parameter) on skin friction coefficient and heat transfer rate, respectively. The threshold line (red dashed line at 2.23 in Figures 1 and at 2.2 in Figure 2) indicates statistical significance at $\alpha = 0.05$. Any factor that

exceeds this threshold implies a significant impact on the responses. Based on Figure 1, the dominant factor influencing the skin friction coefficient is factor *B*, showing the highest standardized effect, followed by factors *A* and *C*, respectively. In addition, factor *B* has the highest influence, suggesting that the changes in this factor will result in the most substantial variations in the skin friction coefficient. Unlike the skin friction coefficient, the heat transfer rate in Figure 2 is most significantly influenced by parameter *C*, with an extremely high standardized effect compared to other factors. Physically, velocity slip (factor *C*) has the most significant effect on reducing/affecting heat transfer rate because it weakens fluid-wall interaction, thickens the thermal boundary layer, and lowers convective heat transport efficiency. Since heat transfer depends on how well thermal energy moves from the surface into the fluid, any disruption caused by slip leads to a noticeable reduction in heat transfer performance.

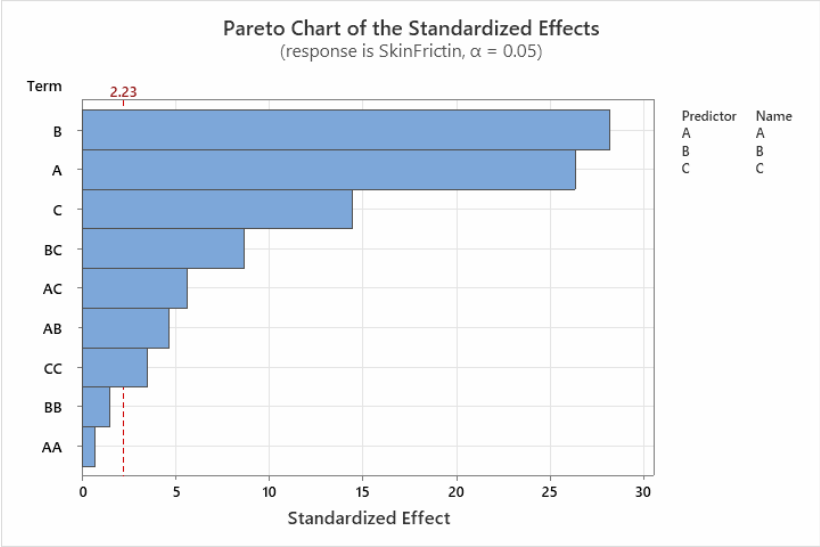

Figure 1. Impact of the evaluated parameters using statistical data analysis on skin friction coefficient.

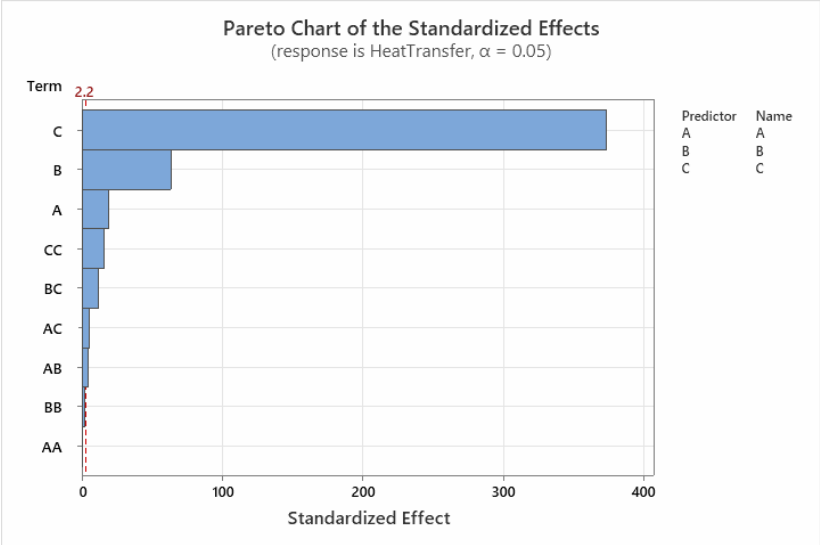

Figure 2. Impact of the evaluated parameters using statistical data analysis on heat transfer rate.

The models for the responses are given by the regression equations

$$y_{\text{skin friction}} = 5.25897 + 0.10146A - 0.10864B + 0.05556C - 0.00522A^2 - 0.01112B^2 - 0.02560C^2 + 0.02012AB + 0.02423AC - 0.03728BC, \quad (11)$$

$$y_{\text{heat transfer}} = 16.8303 + 0.007992A - 0.026554B - 0.156282C - 0.000497A^2 - 0.001395B^2 - 0.012735C^2 + 0.001988AB + 0.002443AC - 0.005624BC. \quad (12)$$

The sensitivity analysis is formulated by partially differentiating the response function from equations (11) and (12), resulting in the sensitivity functions expressed in equations (13) and (14).

$$\frac{\partial(y_{\text{skin friction}})}{\partial A} = 0.10146 + 0.01044A + 0.02012B + 0.02423C,$$

$$\frac{\partial(y_{\text{skin friction}})}{\partial B} = 0.10864 - 0.02224\,B + 0.02012\,A - 0.03728\,C,$$

$$\frac{\partial(y_{\text{skin friction}})}{\partial C} = 0.05556 + 0.0512\,C + 0.02423\,A - 0.03728\,B, \quad (13)$$

$$\frac{\partial(y_{\text{heat transfer}})}{\partial A} = 0.007992 + 0.000994\,A + 0.001988\,B + 0.002443\,C,$$

$$\frac{\partial(y_{\text{heat transfer}})}{\partial B} = 0.026554 - 0.00279\,B + 0.001988\,A - 0.005624\,C,$$

$$\frac{\partial(y_{\text{heat transfer}})}{\partial C} = 0.156282 - 0.02547\,C + 0.002443\,A - 0.005624\,B. \quad (14)$$

Table 3. Analysis of variance (ANOVA) for skin friction

Source	DF	Adj SS	Adj MS	*F*-value	*P*-value
A	1	0.102935	0.102935	692.92	0.000
B	1	0.118031	0.118031	794.54	0.000
C	1	0.030864	0.030864	207.76	0.000
AA	1	0.000075	0.000075	0.50	0.494
BB	1	0.000340	0.000340	2.29	0.161
CC	1	0.001802	0.001802	12.13	0.006
AB	1	0.003238	0.003238	21.79	0.001
AC	1	0.004696	0.004696	31.61	0.000
BC	1	0.011118	0.011118	74.84	0.000
Error	10	0.001486	0.000149		
Lack-of-Fit	5	0.001486	0.000297	*	*
Pure Error	5	0.000000	0.000000		
Total	19	0.279255			

The ANOVA results in Table 3 indicate that parameters A, B, and C, along with their interaction effects, are statistically significant $(p < 0.01)$, demonstrating their substantial influence on skin friction variation. Conversely, the non-significant terms (AA and BB), with high p-values, contribute negligibly and can be omitted from further analysis. These

findings align with the Pareto charts in Figure 1, where factor *B* (curvature parameter) exerts the strongest influence on skin friction, with factors *A* and *C* also playing significant roles. To further enhance sensitivity analysis, factor *A* can be held constant, allowing a more detailed examination of how *B* and *C*, along with their interactions, impact skin friction behavior. There is a significant interaction between factors *B* and *C* in influencing skin friction (Response 1) as shown in Figure 3. In the upper section of the plot, it is observed that for factor *B* at levels -1 and 1, skin friction increases as factor *C* increases from -1 to 1. However, when factor *B* is at level 0, the response remains nearly constant across different levels of factor *C*, indicating that factor *B* significantly impacts how factor *C* affects skin friction. In the lower section, the variation in skin friction with respect to factor *B*, broken down by factor *C*, shows that skin friction decreases as factor *B* increases from -1 to 1, particularly when factor *C* is at levels -1 and 1. This highlights that factor *B* has a pronounced effect on skin friction at these levels of factor *C*, whereas the effect is less significant when factor *C* is at 0. The non-parallel lines across the different levels of factors *B* and *C* suggest a clear interaction between these two factors. Their combined effects on skin friction are not simply additive, and the pattern varies significantly depending on the levels of each factor. This interaction is most evident when factor *C* is at -1 or 1, underscoring the importance of considering both factors together in sensitivity analysis and optimization processes.

Table 4. Analysis of variance for heat transfer

Source	DF	Adj SS	Adj MS	*F*-value	*P*-value
A	1	0.000639	0.000639	363.38	0.000
B	1	0.007051	0.007051	4012.10	0.000
C	1	0.244240	0.244240	138968.52	0.000
AA	1	0.000001	0.000001	0.39	0.548
BB	1	0.000005	0.000005	3.04	0.112
CC	1	0.000446	0.000446	253.75	0.000
AB	1	0.000032	0.000032	17.99	0.002
AC	1	0.000048	0.000048	27.16	0.000
BC	1	0.000253	0.000253	143.95	0.000

Error	10	0.000018	0.000002		
Lack-of-Fit	5	0.000018	0.000004	*	*
Pure Error	5	0.000000	0.000000		
Total	19	0.253250			

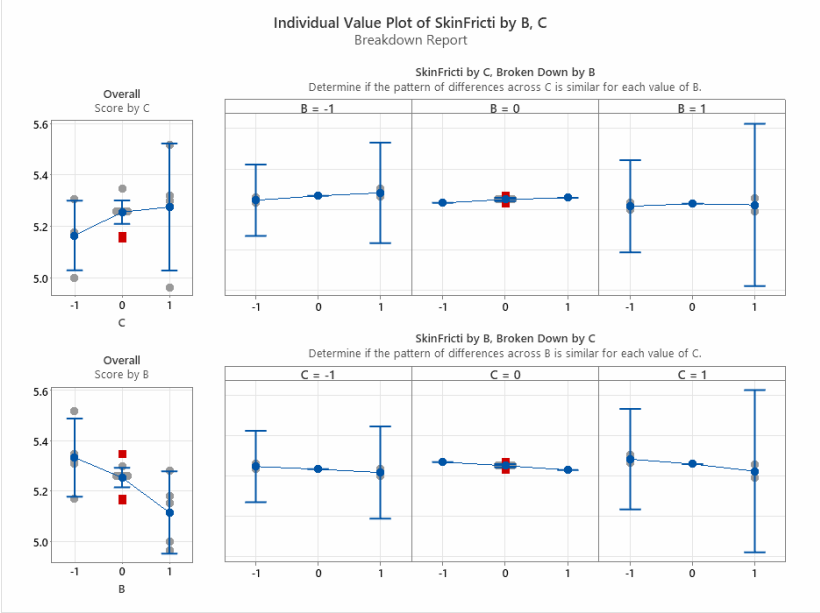

Figure 3. Sensitivity analysis of A, B and C to skin friction.

Based on the ANOVA results in Table 4, it is shown that factors A, B, C, and their interactions (AB, AC, BC, CC) are statistically significant $(p < 0.01)$ and contribute to the variation in heat transfer. Factor C has the most significant influence, as evidenced by its very high F-value (138968.52) and a p-value of 0.000. Factors A and B also significantly affect the response, with p-values of 0.000 and 0.000, respectively, though their influence is smaller compared to factor C. Non-significant terms like AA $(p = 0.548)$ and BB $(p = 0.112)$ can be excluded from further analysis. The model explains the variation in heat transfer well, as indicated by the small error term relative to the total variation (Error SS = 0.000018). This suggests a good fit of the model to the data. The interaction between factors B and C

$(B * C)$ has a particularly strong influence $(p = 0.000)$, suggesting that the combined effect of these two factors plays a significant role in determining heat transfer. For further sensitivity analysis, factors *A* and *C* can be explored more closely, with factor *B* held constant to isolate the effects of *A* and *C* on the response. Based on the analysis of Figure 4, it is evident that there is a significant interaction between factors *A* and *C* in influencing heat transfer (Response 2). In the upper section of the plot, for factor *A* at levels -1 and 1, heat transfer decreases as factor *C* increases from -1 to 1. However, when factor *A* is at level 0, the response remains constant across different levels of factor *C*, indicating that factor *A* has minimal impact on heat transfer at this level of factor *C*. In the lower section of the plot, the variation in heat transfer with respect to factor *A*, broken down by factor *C*, shows that heat transfer decreases as factor *A* increases from -1 to 1 when factor *C* is at -1. When factor *C* is at 0, there is no significant change in heat transfer across different levels of factor *A*. However, when factor *C* is at 1, heat transfer increases as factor *A* increases, suggesting that factor *A* has a positive effect on heat transfer at this level of factor *C*. The non-parallel lines across the different levels of factors *A* and *C* highlight a significant interaction between these factors, indicating that their combined effects on heat transfer are not simply additive. This interaction is most pronounced when factor *C* is at levels -1 or 1, where the effect of factor *A* on heat transfer is more noticeable. When factor *C* is at 0, the effect of factor *A* is minimal, suggesting that factor *A*'s impact is sensitive to the levels of factor *C*. Therefore, it is important to consider both factors *A* and *C* together in sensitivity analysis, as their combined effects on heat transfer are more complex than their individual impacts. Further investigation into the interaction between these factors, particularly at the extreme levels of factor *C*, could provide valuable insights for optimizing heat transfer.

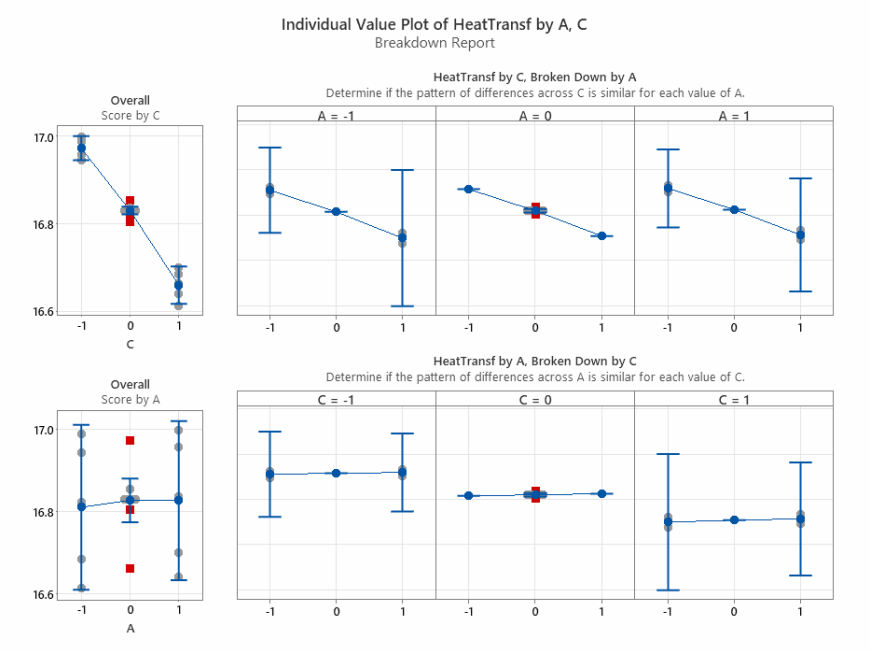

Figure 4. Sensitivity analysis of A, B and C to heat transfer.

4. Conclusions

This study presents a comprehensive analysis of ternary hybrid nanofluid flow over a permeable cylinder, investigating the effects of magnetic field, curvature, and velocity slip on skin friction and heat transfer characteristics. The findings indicate that velocity slip parameter (factor C) has the most significant impact on heat transfer enhancement, as it directly influences the thermal boundary layer structure and energy dissipation at the surface. Meanwhile, curvature parameter (factor B) is identified as the dominant factor in determining the skin friction coefficient, highlighting its role in shaping flow resistance and boundary layer characteristics. The ANOVA results further confirm that interaction effects, particularly BC and AC, contribute significantly to variations in the response variables, suggesting that optimizing these parameters can lead to improved flow stability and heat transfer efficiency.

Acknowledgements

We acknowledge research support from Universiti Teknikal Malaysia Melaka, Malaysia through international research matching grant: ANTARABANGSA(IRMG)-TEL-U/2025/FTKM/A00086.

References

[1] M. A. Sheremet, D. S. Cimpean and I. Pop, Thermogravitational convection of hybrid nanofluid in a porous chamber with a central heat-conducting body, Symmetry 12(4) (2020), 593.

[2] M. A. Sheremet, T. Grosan and I. Pop, MHD free convection flow in an inclined square cavity filled with both nanofluids and gyrotactic microorganisms, International Journal of Numerical Methods for Heat and Fluid Flow 29(12) (2019), 4642-4659.

[3] M. A. Sheremet, T. Grosan and I. Pop, Thermal convection in a chamber filled with a nanosuspension driven by a chemical reaction using Tiwari and Das' model, International Journal of Numerical Methods for Heat and Fluid Flow 31(1) (2021), 452-470.

[4] H. Babazadeh, M. A. Sheremet, H. A. Mohammed, M. R. Hajizadeh and Z. Li, Inclusion of nanoparticles in PCM for heat release unit, Journal of Molecular Liquids 313 (2020), 113544.

[5] X. Zhang, M. Sheikholeslami, M. Jafaryar, M. A. Sheremet, A. Shafee and H. Babazadeh, Simulation for melting of paraffin for saving energy with utilize of nanoparticles, Journal of Molecular Liquids 313 (2020), 113574.

[6] S. A. Devi and S. S. U. Devi, Numerical investigation of hydromagnetic hybrid Cu-Al_2O_3/water nanofluid flow over a permeable stretching sheet with suction, International Journal of Nonlinear Sciences and Numerical Simulation 17(5) (2016), 249-257.

[7] S. S. U. Devi and S. A. Devi, Numerical investigation of three-dimensional hybrid Cu-Al_2O_3/water nanofluid flow over a stretching sheet with effecting Lorentz force subject to Newtonian heating, Canadian Journal of Physics 94(5) (2016), 490-496.

[8] S. S. U. Devi and S. A. Devi, Heat transfer enhancement of Cu-Al_2O_3/water hybrid nanofluid flow over a stretching sheet, Journal of the Nigerian Mathematical Society 36(2) (2017), 419-433.

[9] B. Takabi and S. Salehi, Augmentation of the heat transfer performance of a sinusoidal corrugated enclosure by employing hybrid nanofluid, Advances in Mechanical Engineering 6 (2014), 147059.

[10] J. Sarkar, P. Ghosh and A. Adil, A review on hybrid nanofluids: recent research, development and applications, Renewable and Sustainable Energy Reviews 43 (2015), 164-177.

[11] N. A. Sidik, I. M. Adamu, M. M. Jamil, G. H. Kefayati, R. Mamat and G. Najafi, Recent progress on hybrid nanofluids in heat transfer applications: a comprehensive review, International Communications in Heat and Mass Transfer 78 (2016), 68-79.

[12] L. S. Sundar, K. V. Sharma, M. K. Singh and A. C. Sousa, Hybrid nanofluids preparation, thermal properties, heat transfer and friction factor-a review, Renewable and Sustainable Energy Reviews 68 (2017), 185-198.

[13] J. R. Babu, K. K. Kumar and S. S. Rao, State-of-art review on hybrid nanofluids, Renewable and Sustainable Energy Reviews 77 (2017), 551-565.

[14] M. U. Sajid and H. M. Ali, Thermal conductivity of hybrid nanofluids: a critical review, International Journal of Heat and Mass Transfer 126 (2018), 211-234.

[15] F. N. Jamrus, I. Waini, U. Khan and A. Ishak, Effects of magnetohydrodynamics and velocity slip on mixed convective flow of thermally stratified ternary hybrid nanofluid over a stretching/shrinking sheet, Case Studies in Thermal Engineering 55 (2024), 104161.

[16] F. N. Jamrus, A. Ishak, I. Waini, U. Khan, M. I. Siddiqui and J. K. Madhukesh, Aspects of non-unique solutions for Hiemenz flow filled with ternary hybrid nanofluid over a stretching/shrinking sheet, Advances in Mathematical Physics 2024(1) (2024), 7253630.

[17] U. N. Hussein, N. S. Khashi'ie, N. M. Arifin and I. Pop, Magnetohydrodynamics (MHD) flow of ternary nanofluid and heat transfer past a permeable cylinder with velocity slip, Chinese Journal of Physics 93 (2025), 328-339.

[18] U. N. Hussein, N. S. Khashi'ie, K. B. Hamzah, N. M. Arifin and I. Pop, Joule heating effect on ternary nanofluid flow and heat transfer over a permeable cylinder, JP Journal of Heat and Mass Transfer 37(6) (2024), 831-841.

[19] T. Mehmood, M. Ramzan, F. Howari, S. Kadry and Y. M. Chu, Application of response surface methodology on the nanofluid flow over a rotating disk with autocatalytic chemical reaction and entropy generation optimization, Scientific Reports 11(1) (2021), 4021.

[20] B. Mahanthesh and K. Thriveni, Nanoparticle aggregation effects on radiative heat transport of nanoliquid over a vertical cylinder with sensitivity analysis, Applied Mathematics and Mechanics 42(3) (2021), 331-346.

[21] S. M. Vahedi, A. Z. Ghadi and M. S. Valipour, Application of response surface methodology in the optimization of magneto-hydrodynamic flow around and through a porous circular cylinder, Journal of Mechanics 34(5) (2018), 695-710.

[22] Z. Abdelmalek, B. Mahanthesh, M. F. Basir, M. Imtiaz, J. Mackolil, N. S. Khan, H. A. Nabwey and I. Tlili, Mixed radiated magneto Casson fluid flow with Arrhenius activation energy and Newtonian heating effects: Flow and sensitivity analysis, Alexandria Engineering Journal 59(5) (2020), 3991-4011.

[23] R. K. Tiwari and M. K. Das, Heat transfer augmentation in a two-sided lid-driven differentially heated square cavity utilizing nanofluids, International Journal of Heat and Mass Transfer 50(9-10) (2007), 2002-2018.